

The significance of early and late stages of coupled aggregation and sedimentation in the fate of nanoparticles: measurement and modelling

BABAKHANI, Peyman, DOONG, Ruey-an and BRIDGE, Jonathan
<<http://orcid.org/0000-0003-3717-519X>>

Available from Sheffield Hallam University Research Archive (SHURA) at:
<https://shura.shu.ac.uk/21922/>

This document is the Accepted Version [AM]

Citation:

BABAKHANI, Peyman, DOONG, Ruey-an and BRIDGE, Jonathan (2018). The significance of early and late stages of coupled aggregation and sedimentation in the fate of nanoparticles: measurement and modelling. *Environmental Science & Technology*, 52 (15), 8419-8428. [Article]

Copyright and re-use policy

See <http://shura.shu.ac.uk/information.html>

Environmental Modeling

The significance of early and late stages of coupled aggregation and sedimentation in the fate of nanoparticles: measurement and modelling

Peyman Babakhani, Ruey-an Doong, and Jonathan Bridge

Environ. Sci. Technol., **Just Accepted Manuscript** • DOI: 10.1021/acs.est.7b05236 • Publication Date (Web): 05 Jul 2018Downloaded from <http://pubs.acs.org> on July 11, 2018

Just Accepted

"Just Accepted" manuscripts have been peer-reviewed and accepted for publication. They are posted online prior to technical editing, formatting for publication and author proofing. The American Chemical Society provides "Just Accepted" as a service to the research community to expedite the dissemination of scientific material as soon as possible after acceptance. "Just Accepted" manuscripts appear in full in PDF format accompanied by an HTML abstract. "Just Accepted" manuscripts have been fully peer reviewed, but should not be considered the official version of record. They are citable by the Digital Object Identifier (DOI®). "Just Accepted" is an optional service offered to authors. Therefore, the "Just Accepted" Web site may not include all articles that will be published in the journal. After a manuscript is technically edited and formatted, it will be removed from the "Just Accepted" Web site and published as an ASAP article. Note that technical editing may introduce minor changes to the manuscript text and/or graphics which could affect content, and all legal disclaimers and ethical guidelines that apply to the journal pertain. ACS cannot be held responsible for errors or consequences arising from the use of information contained in these "Just Accepted" manuscripts.

The significance of early and late stages of coupled aggregation and sedimentation in the fate of nanoparticles: measurement and modelling

Peyman Babakhani^{1,2}, Ruey-an Doong^{2,3}, Jonathan Bridge^{4}*

¹Department of Civil Engineering and Industrial Design, University of Liverpool, Liverpool, Merseyside L69 7ZX, UK

²Department of Biomedical Engineering and Environmental Sciences, National Tsing Hua University, No. 101, Section 2, Kuang Fu Road, Hsinchu, 30013, Taiwan

³Institute of Environmental Engineering, National Chiao Tung University, No. 1001, University Road, Hsinchu, 30010, Taiwan

⁴Department of the Natural and Built Environment, Sheffield Hallam University, Howard St, Sheffield S1 1WB, UK.

*Corresponding author:

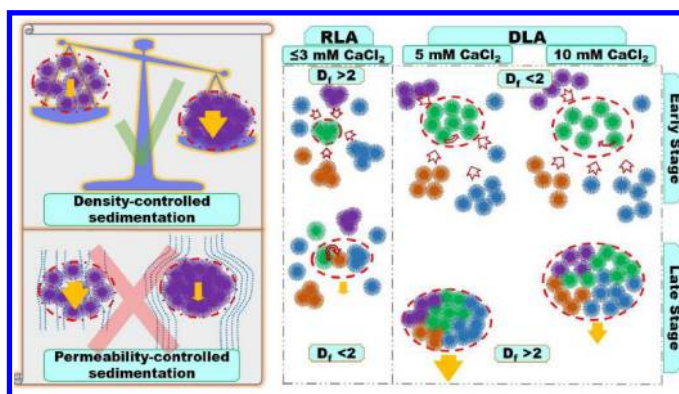
Jonathan Bridge

T +44(0)114 225 5144

Email j.w.bridge@shu.ac.uk

Abstract.

Despite aggregation's crucial role in controlling the environmental fate of nanoparticles (NP), the extent to which current models can describe the progressive stages of NP



aggregation/sedimentation is still unclear. In this paper, 24 model combinations of two population-balance models (PBMs) and various collision frequency and settling velocity models are used to analyse spatiotemporal variations in the size and concentration of hydroxyapatite (HAp) NP. The impact of initial conditions and variability in attachment efficiency, α , with aggregate size are investigated. Although permeability models perform well in calculating collision frequencies, they are not appropriate for describing settling velocity because of their negative correlation or insensitivity in respect to fractal dimension. Considering both early and late stages of aggregation, both experimental and model data indicate overall mass removal peaks at an intermediate ionic strength (5 mM CaCl₂) even though the mean aggregate size continued to increase through higher ionic strengths (to 10 mM CaCl₂). This trend was consistent when different approaches to the initial particle size distribution (PSD) were used and when a variable or constant α was used. These results point to the importance of accurately considering different stages of aggregation in modeling NP fate within various environmental conditions.

Keywords: nanoparticles; early and late stage aggregation; sedimentation; population balance modelling; fractal dimension; settling velocity

44 **Nomenclature**

45	a_0	primary particle radius or particle radius in the smallest size class [L]
46	a_k	aggregate radius in size class k [L]
47	D_f	fractal dimension [–]
48	D_H	hydrodynamic diameter
49	G	shear rate [T^{-1}]
50	i, j	subscripts used to indicate aggregates size class i and j
51	k_b	Boltzmann constant
52	k_{max}	maximum number of classes considered in the numerical model (<100)
53	n_k	aggregate number concentration in size class k [L^{-3}]
54	q	geometric factor
55	T	temperature [K]
56	U_k	aggregate sedimentation velocity in size class k [LT^{-1}]
57	U_0	sedimentation velocity of primary particles [LT^{-1}]
58	v_k	volume of solids of each aggregate in size class k [L^3]
59	v_0	volume of primary particles [L^3]
60	Z_s	sedimentation depth [L]

- 61 α attachment efficiency [–]
- 62 $\beta_{i,j}$ aggregate collision frequency in size class i and j [L^3T^{-1}]
- 63 β_{Diff} differential settling collision frequency [L^3T^{-1}]
- 64 β_{Orth} orthokinetic collision frequency [L^3T^{-1}]
- 65 β_{Prik} perikinetic collision frequency [L^3T^{-1}]
- 66 $\delta_{j,i}$ Kronecker delta
- 67 μ dynamic viscosity of the suspending medium [$M T^{-1} L^{-1}$]
- 68 **List of abbreviations.**
- 69 CCC critical coagulation concentration
- 70 DCR derived count rate
- 71 DI deionized
- 72 DLA diffusion limited aggregation
- 73 DLS dynamic light scattering
- 74 DLVO Derjaguin, Landau, Verwey, and Overbeek
- 75 FP fixed pivot
- 76 HAp hydroxyapatite
- 77 IS ionic strength

78	MP	moving pivot
79	NP	nanoparticles
80	PB	population balance
81	PSD	particle size distribution
82	RLA	reaction limited aggregation
83	SI	Supporting Information
84		
85		

Introduction

Nanoparticles, often unintentionally released into the environment, have also shown promise in remediation of hazardous contaminants such as radionuclides.¹⁻³ Effective *in situ* field-scale management of NP is hindered by the lack of adequate models to simulate NP fate and transport in realistic environmental compartments.^{4, 5} Considering the long-established potential for colloids to enhance the mobility of contaminants in groundwater environments^{6, 7} or facilitate their redistribution in surface water bodies,⁸⁻¹⁰ this lack of predictive capability is a critical concern. Aggregation of NP is important because progressive increase in particle size can substantially affect NP mobility, reactivity and hence potential contribution to mobilization of other solute contaminants.^{4, 11-13} Aggregation has complex interactions with other NP transport mechanisms such as sedimentation.^{4, 5, 14, 15} This leads to distinct changes in trends of particle concentration or size over time.^{14, 16} The early stage of aggregation, in which the slope of mean particle size versus time is typically linear, is the subject of many studies.^{15, 17, 18} However, the late stage of aggregation, more common in environmentally-relevant conditions where phenomena such as aggregation and sedimentation occur over longer periods with no clear initial condition, has received relatively little attention to date.^{14, 16}

In late-stage conditions, NP aggregate sizes increase sufficiently to induce sedimentation and removal from suspension. This may lead to decreasing concentration of NP dispersion and consequently reduction in aggregation rates. Conversely, differentially-settling aggregates may collect smaller particles more easily during late-stage. Sedimentation-induced movement of aggregates may bring about aggregate restructuring.¹⁹ This may affect the number of collisions among aggregates thereby changing their consequent aggregation rates and settling velocity.^{19, 20} These complex interacting phenomena may drive localised nonlinearities in slope of mean particle size or concentration versus time. Many established theories and concepts, such as

CCC, are invalidated during late-stage aggregation since they are based upon the linear slope of size or concentration versus time at the early stage.^{21, 22}

The ability of PB models to account for both stages in tandem while retaining meaningful description of the system in terms of parameters such as attachment efficiency, α , and fractal dimension, D_f is still unclear but is important if PB approaches are to be used to provide description of aggregation processes within larger-scale models of NP fate and transport.^{20, 23}

In this study, we measure and model the quiescent aggregation and sedimentation of HAp NP across a range of solution chemistries and at different measurement depths over a period of at least five hours—sufficient in most of the cases for systems to develop late stage conditions.

We systematically investigate two numerical approaches to aggregation combined with different settling velocity and collision frequency terms to find the models which best describe observed mean particle size, averaged concentration, and PSD. Using the best-performing model set, we then investigate how the trends of parameters change from early-stage to early-late-stage cases across a range of solution chemistries and at different positions within a short column. The initial PSD is a critical variable in aggregation modelling. We applied models with three approaches: initial PSD observed in each experiment as the initial condition in each model (A); constant initial condition for all experiments/models (B); and the latter approach with variable- α across different size classes, accounting for aggregate size-driven variations in surface interaction energy profiles according to the DLVO theory (C).²⁴ This comprehensive experimental and numerical study yields new insights into both the changing dynamics of aggregation as NP systems evolve over time, and the applicability of model concepts used to describe them.

Modelling

Population balance models such as the Smoluchowski model^{25, 26} are the most widely-used methods for predicting aggregation-driven PSD of colloidal suspensions.²⁷⁻²⁹ However, the basic discretised form of these models applies only when each aggregate size class volume is considered the arithmetic sum of volumes of smaller classes. To span the size range that can result from early and late stages of aggregation, e.g., 40 nm to 10 μm , over 10^5 size classes are required, for each of which the PB equation should be solved. This is computationally impractical, particularly when other transport phenomena are modelled or for iterative calibration of parameters against experimental data. A geometric size discretization technique proposed^{30, 31} to mitigate this issue was recently used by Dale et al.³² to simulate aggregation and dissolution of environmentally-relevant NP. A geometric series of aggregate volumes is given as $v_{i+1}/v_i = 2^{1/q}$, where q is an integer greater than or equal to one. However, values of q derived from PSD obtained from experimental techniques such as DLS are typically non-integer, e.g., varying from $q = 1.574$ for $D_f = 3$ to $q = 2.63$ for $D_f = 1.8$.

More flexible approaches include FP and MP techniques.^{33, 34} Fixed-pivot maintains a minimum number of size classes (bins) via selective refinement of a coarse discretization of the particle volume dimension. This approach can consider binary or multiple collisions. Ignoring terms for breakage and adding a sedimentation term, the FP model conserving two properties of mass and number can be expressed as:³³

$$\frac{dn_k}{dt} = \sum_{\substack{j \geq i \\ v_{k-1} \leq (v_j + v_i) \leq v_{k+1}}} \left[1 - \frac{1}{2} \delta_{j,i} \right] \eta_k \alpha_{j,i} \beta_{j,i} n_j n_i - n_k \sum_{i=1}^{k_{\max}} \alpha_{k,i} \beta_{k,i} n_i - \frac{U_k}{Z_s} n_k \quad (1)$$

where η_k is given as:

$$\eta_k = \begin{cases} \frac{v_{k+1} - (v_j + v_i)}{v_{k+1} - v_k}, & v_k \leq (v_j + v_i) \leq v_{k+1} \\ \frac{(v_j + v_i) - v_{k-1}}{v_k - v_{k-1}}, & v_{k-1} \leq (v_j + v_i) \leq v_k \end{cases} \quad (2)$$

152 The MP model³⁴ assumes that when the particle number concentration in a size class changes
 153 from sharp-decreasing gradients toward near-uniformity, the 'pivot' (the representative point of
 154 each size class in the particle size distribution) moves from the lower end of that class toward
 155 the middle. Two differential equations need to be solved over time. Omitting the breakage-
 156 relevant terms and considering the sedimentation term, the governing equations for the MP
 157 model become:

$$\frac{dn_k}{dt} = \sum_{\substack{j \geq i \\ v_k \leq (v_j + v_i) \leq v_{k+1}}} \left[1 - \frac{1}{2} \delta_{j,i} \right] \alpha_{j,i} \beta_{j,i} n_j n_i - n_k \sum_{i=1}^{k_{max}} \alpha_{k,i} \beta_{k,i} n_i - \frac{U_k}{Z_s} n_k \quad (3)$$

$$\frac{dv_k}{dt} = \frac{1}{n_k} \sum_{\substack{j \geq i \\ v_k \leq (v_j + v_i) \leq v_{k+1}}} \left[1 - \frac{1}{2} \delta_{j,i} \right] [(v_j + v_i) - v_k] \alpha_{j,i} \beta_{j,i} n_j n_i \quad (4)$$

158 Equations (1-4) can be solved for a given initial PSD, to yield PSDs resulting from aggregation
 159 and sedimentation at any time for a specified sedimentation depth Z_s . From the PSD, other
 160 quantities such as mean D_H and mass concentration can be determined as described in the SI.
 161 Note that, following common practice in this area,³⁵⁻³⁷ sedimentation is not modelled as a mass
 162 transfer process but as a net mass loss rate for each size class which scales linearly with Z_s .

163 The collision frequency for environmental colloids is commonly given as the sum of three
 164 mechanisms: perikinetic collisions (Brownian), orthokinetic collisions (shear-induced

aggregation under fluid motion), and differential settling (collection of smaller aggregates by the larger ones during sedimentation).¹⁷ Expressing collision frequencies based on the volume (or mass) of aggregates as a representative variable,^{32, 38} using fractal dimension relationships and considering permeability drag effects,³⁹ the following relationships yield:

$$\beta_{Prik_{i,j}} = \frac{2k_b T}{3\mu} \left(v_i^{\left(\frac{1}{D_f}\right)} + v_j^{\left(\frac{1}{D_f}\right)} \right) \left(\frac{1}{\Omega_i} v_i^{-\left(\frac{1}{D_f}\right)} + \frac{1}{\Omega_j} v_j^{-\left(\frac{1}{D_f}\right)} \right) \quad (5)$$

$$\beta_{Orth_{i,j}} = \frac{G}{\pi} v_0^{\left(1-\frac{3}{D_f}\right)} \left(\left(\eta_{c_i}^{\left(\frac{1}{2}\right)} v_i^{\left(\frac{1}{D_f}\right)} + \eta_{c_j}^{\left(\frac{1}{2}\right)} v_j^{\left(\frac{1}{D_f}\right)} \right)^3 \right) \quad (6)$$

$$\beta_{Diff_{i,j}} = \frac{3}{2} \left(\frac{\pi}{6} \right)^{\frac{1}{3}} v_0^{\left(\frac{2}{3}-\frac{2}{D_f}\right)} \left(\eta_{c_i}^{\left(\frac{1}{2}\right)} v_i^{\left(\frac{1}{D_f}\right)} + \eta_{c_j}^{\left(\frac{1}{2}\right)} v_j^{\left(\frac{1}{D_f}\right)} \right)^2 |U_i - U_j| \quad (7)$$

The superposition of the three rates gives the total rate of collisions, $\beta(i, j)$:

$$\beta_{i,j} = \beta_{Prik_{i,j}} + \beta_{Orth_{i,j}} + \beta_{Diff_{i,j}} \quad (8)$$

where Ω is the drag coefficient correction factor defined as the ratio of drag force exerted on a permeable aggregate to drag force exerted on an impervious aggregate with the same size,^{35, 40} and η_c is the fluid collection efficiency of an aggregate, defined as the ratio of flow through an aggregate to total flow approaching the aggregate.^{35, 41} To calculate collision frequencies, we use two permeability models: the Brinkman permeability model^{35, 42} and the Davies permeability model.⁴³ Additionally, we investigate the use of collision frequencies calculated based only on fractal relationships without permeability consideration.^{44, 45} Four types of settling velocity models were investigated for NP aggregates of fractal nature. These include an empirical power-law equation,^{46, 47} a permeability model based on the Davies correlation,^{43,}⁴⁸ a permeability model based on the Brinkman model,^{35, 40, 41} and a fractal model which considers the effect of the size distribution of primary particles forming each aggregate.^{49, 50}

Finally, in the variable α approach, α was calculated based on DLVO theory considering only van der Waals attraction and electrostatic repulsion interaction energies. The Hamaker constant for HAp-water-HAp system was calculated as 2.77×10^{-21} J.⁵¹ All models and their related equations are thoroughly introduced in the SI.

Materials and Methods

Numerical modelling

Details of MATLAB® (Mathworks, USA) codes for all models used in this study are available in the SI. In brief, an explicit forward Euler scheme was used for the time derivative. The explicit approach was chosen due to potential inaccuracy and computational problems of using an iterative implicit approach.⁵² A simple forward Euler approach was selected since higher-order schemes, such as fourth-order Runge-Kutta, were previously found ineffective in solving PB models, which are examples of “stiff” problems.^{32, 53} Potential numerical instability in certain ranges of parameters within the explicit model was mitigated by an adjustable time step and a novel optimization algorithm based on a heuristic approach which, by incrementing a parameter at a time within set ranges, enhanced the fit between observations and model outputs using a parallel processing approach. An automatic increase of initial time step of the ‘slave’ numerical model by the ‘master’ optimization algorithm helped prevent unstable runs affecting the optimization process.

Parameter calibration was conducted on the Chadwick high performance cluster and the Condor high throughput computational systems at the University of Liverpool. Comparison of numerical model performance with analytical solutions of the Smoluchowski model for both monodisperse¹⁷ and log-normal-distributed initial conditions⁵⁴ is demonstrated in the SI. The Nash–Sutcliffe determination coefficient (a conservative R^2)⁵⁵ was used to assess goodness of

fit. In this study, we calibrated the parameters based on the hydrodynamic size as an objective function and investigate how well the fitted model describes concentration variation over time and PSD at certain times.

Experiment procedure

Hydroxyapatite (particle density = 3.16 g/cm³) was obtained from Alfa Aesar, UK. Evolution of aggregate mean size, PSD and concentration over time were measured by DLS (Malvern Zetasizer Nano ZS, UK). The valid measurement size range reported by the manufacturer is from 1 nm to 10⁴ nm. Measurements were carried out with an interval of ~3.37 min. For all measurements, the number of runs was 5 (duration 10 s), beam attenuator index was 11, position of measurement was 6.5 mm following pre-tests to establish the least noise and highest reproducibility in the count rate as well as the Z-average data (hydrodynamic diameter, D_H). Zeta potential was measured with the same instrument with an automatic adjustment. To prevent the growth of bacteria in samples during the course of the experiment, we added 10 mM sodium azide. This was also beneficial due to its buffering capability to ensure a stable pH, although corollary measurements indicated a potential variation of ± 0.52 at pH 7-10 over 24 h.

All experiments were conducted for at least 5 hours and in duplicate according to this procedure: (1) prepare particle dispersion in DI water with a final particle concentration 50 mg/L, and sodium azide concentration 10 mM; (2) adjust pH at 6, 7, 10, or 11 \pm 0.05 with NaOH/HCl (100 mM); (3) ultrasonicate 5 min, add electrolyte (CaCl₂) to reach concentrations of 0, 1, 2.5, 3, 5, 7.5, 10 mM, immediately vortex 5 sec, transfer to a disposable cuvette and immediately start the DLS measurement. The whole process duration, from ultrasonication until the start of the first measurement, was 70 \pm 20 sec. Standard sample volume of 3 mL resulted in a measurement depth of ~2.33 cm. We also investigated the impact of the

measurement depth by varying the sample volume as 1 mL, 3 mL, and 4 mL, corresponding to approximate measurement depths of 0.33 cm, 2.33 cm, and 3.33 cm, respectively. The DCR, which is the measured DLS count rate divided by the attenuation factor was extracted from the DLS data and used as an indicator of mass concentration.⁵⁶⁻⁵⁸ To assess the significance of the relationship between DCR and the mass concentration, DCR was measured at different concentrations (1, 5, 10, 50, 100, 250, and 500 mg/L) of HAp NP.

Results and Discussion

Experimental results

Figure 1 shows averaged D_H and DCR for HAp at various solution chemistries over 5 hours. DLS measurements of aggregate D_H evolution showed low noise and good reproducibility as indicated by small standard deviations of duplicate experiments (error bars, Fig. 1). However, stability of DCR measurements tended to decrease over time. At constant pH 6, below 3 mM CaCl_2 the slope of D_H versus time is near linear on a semi-log plot throughout the experiment; above 3 mM the slope asymptotes from a steep slope at < 40 min to a gentle slope at greater times, revealing both early and late stages of aggregation/sedimentation (Fig. 1a). This also suggests that the CCC lies between 3 and 5 mM CaCl_2 . Similar behaviour is observed for various pH when the ionic strength is held at 5 mM CaCl_2 (Fig. 1b). Figures 1c,d illustrate DCR data normalized to the initial DCR value of each experiment. This quantity drops below 0.5 by the end of the experiments in most cases under the DLA regime (>4 mM CaCl_2). However, normalized DCR increases over time for RLA regime (CaCl_2 concentrations < 4 mM). This increasing trend might be interpreted as settling, slow-aggregating particles arriving at the point of measurement from further up the water column, causing increase of mass concentration in this point to above the initial uniform concentration in the sample. Such an increased concentration in the lower positions of the water column has been already reported.⁵⁹⁻

⁶¹ Although DCR data have been used as proxy for colloid mass concentration in multiple studies,^{57, 58, 62, 63} its application in NP studies is less common,⁵⁶ and there have been indications that DCR can be affected by size⁶⁴ or the number of particles⁶¹ in addition to the mass. We assessed the relationship between the DCR and HAp concentration in the ranges 1 to 100, 250, or 500 mg/L in DI water. The result of this investigation revealed a linear correlation ($r^2 > 0.98$ and $P \gg 0.05$) between these two factors (Fig. S1, SI). We should note that the use of DLS data like any experimental technique has inherent measurement uncertainties, e.g., mean hydrodynamic size might be affected by the larger fraction of PSD.⁶⁵ However, as shown in PSD results (Figs. S2 and S3) developing a monodisperse PSD toward later times suggests that this impact might not be significant here.

Model screening

A detailed discussion of the screening of the 24 model combinations is provided as SI (Figs. S4-S6 and Tables S1-S4). Briefly, for both FP and MP models, calculation of collision frequencies using the simple fractal approach or Davies permeability correlation led to poorer matches between the experimental and modelled D_H values (Fig. S4) than when permeability collision frequencies were based on the Brinkman model. In the two former collision models, R^2 of D_H data was below 0.5, whereas for the Brinkman permeability model R^2 increased up to 0.71 (Tables S1 and S2). Fits to DCR data were relatively insensitive to model type (Table S3). The simple fractal and Davies permeability correlation approaches led to D_H curve shapes inconsistent with the experimental data. Therefore, we discarded these two collision frequency models. The best among the settling velocity models, using the FP numerical approach, was the power-law formulation in terms of fitting for D_H data ($R^2 = 0.71$). Using the MP scheme, the power law, Brinkman permeability, and size distribution models gave close fitting results

275 with R^2 equal to 0.68, 0.71, and 0.70, respectively, against D_H data and 0.62, 0.58, and 0.87,
276 respectively against DCR data (Table S2).

277 The FP model performs much faster than the MP method in simulating both early and late
278 stages of aggregation. In fact, once the initial stage of the aggregation is passed, a significant
279 increase (e.g., 500 times) in the time step length can be adopted for the FP model without
280 affecting model stability. The MP method, in spite of being originally faster than FP,⁵³ is not
281 as flexible as FP in reducing the number of time steps in the late stage, potentially because of
282 sharp gradients at longer times caused by the additional volume-based equation in the MP
283 model. The final selected model set (FP, Brinkman-permeability-based collision frequency,
284 and power-law settling velocity) based on a case-specific initial PSD (approach A, Table 1) fit
285 the experimental data with mean R^2 of 0.795 (D_H) and 0.670 (DCR) for all cases with various
286 pH and IS except the cases under the RLA regime (Fig. 1, Table S3). The model matched to
287 D_H data could well describe normalized DCR trends under the DLA condition, suggesting that
288 in this regime DCR is an appropriate representative of mass concentration.

289 *Aggregate structure and sedimentation velocity*

290 The model fit results indicate that models assuming bulk density-controlled sedimentation tend
291 to outperform models assuming permeability-controlled sedimentation. The impact of
292 aggregate structure on settling velocity is a disputed subject.⁶⁶ Enhanced sedimentation
293 velocities compared to Stokes' law based on hydrodynamic size have been reported and
294 interpreted as flow through the aggregates reducing the aggregate drag.^{40, 42, 43, 67} Other
295 studies^{47, 68, 69} point to the overestimation of Stokes' law for floc sedimentation velocity. We
296 compared trends in terminal settling velocity versus the size of aggregates resulted from each
297 sedimentation model used in the present study.

Figure 2 illustrates, for three values of D_f (1.6, 2.0, and 2.3), that the highest sedimentation velocity is predicted by the Davies permeability model, followed by the Brinkman, size-distribution-based and power-law models, respectively. The Davies permeability model predicts an increase in sedimentation velocity with decrease of D_f in agreement with other studies.^{40, 43, 67} However, this model yields an estimate of settling velocity that is much higher than all the other models.⁷⁰ The Brinkman model exhibits a slight increase of velocity with D_f which is only discernible for particles of less than 1 μm in size—not considerable in the sedimentation process.^{17, 71} This low sensitivity of settling velocity to the aggregate structure contradicts experimental observations.^{40, 42, 43, 47, 67, 68} However, both power-law and size-distribution-based models predict increased velocity with D_f due to the greater bulk density of aggregates (Fig. 2). This variation is more significant for the power-law model compared to the size-distribution-based model, suggesting that the power-law expression is more sensitive to D_f . Overall, simulations incorporating these bulk density-controlled sedimentation terms yielded the best fits against our experimental data.

Figure 2 shows that for particles of the same matter and with constant diameter, reducing D_f (i.e. increasing porosity and decreasing mass) results in considerable reduction in the settling velocity according to power-law and size-distribution-based models. Recently, in an insightful study, Emadzadeh and Chiew⁷² showed that for large synthetic particles (> 1 cm in size and density $\gg 1$ g cm⁻³) with identical matter and diameter, increasing porosity corresponding to a decreased mass caused reduction of the terminal settling velocity. However, when particles of different matter were used to maintain the mass constant too, the particles with higher porosity exhibited higher settling velocity. This implies for homogeneous NP aggregates with density of primary particles $\gg 1$ g cm⁻³, the impact of the bulk density of aggregates far outweighs permeability or drag effects, in agreement with our analysis based on best fits to early and late stage HAp aggregation data and in contrast to Johnson et al.⁴³

323 *Attachment efficiency and fractal dimension*

324 Table 1 shows the parameters determined from the fitting (optimisation) procedure,
325 demonstrating that with the increase of CaCl_2 concentration above 5 mM the model parameter
326 α increases above one. Classical theories of aggregation^{18, 22} prescribe that attachment
327 efficiency increases until the double layer repulsion is completely screened, where the CCC is
328 met and α is equal to one. Calculation of DLVO profiles, shown in Fig. S7, confirms that at
329 $[\text{CaCl}_2] \geq 5$ mM there is no energy barrier against aggregation. We interpret values greater
330 than one in this model parameter as indicating a mechanism associated with the late-stage
331 aggregation which enhances the *effective* attachment efficiency above its classical limit.
332 Although there have been cases in the literature reporting α above unity,^{67, 73-76} to investigate
333 this further, we fitted the model to D_H data only at the early stage (first 20 min) of the processes.
334 Since we found including D_f as an estimating parameter was not necessary for early-stage
335 fitting, we fixed this at 1.6 (close to the common DLA range) for all cases of pH and high IS.
336 Results, presented in Table S5, reveal that for most of the cases α reduces to below one. The
337 only remaining case with $\alpha > 1$ also reduces to below one if D_f is considered as a free parameter
338 in the optimization process.

339 To scrutinize this issue further, we fixed the initial PSD in all cases based on a single-peaked
340 PSD extracted from the experimental case with no aggregation (approach B, Table 1). In this
341 approach, the very first moments of the aggregation (~ 70 s), which are not captured in
342 experiments, are considered by the model with shear coagulation operating, and the
343 sedimentation process turned off as described in the SI. This approach yields slightly poorer
344 goodness-of-fit (mean R^2 0.736 for D_H and 0.513 for DCR) than approach A (mean R^2 0.763
345 for D_H and 0.64 for DCR) for cases of $\text{IS} > 5$ mM and various pH (Figs. 1, S8 and Table S3).
346 In contrast to approach A, approach B yields α closer to one in all cases of high IS (maximum

α is 1.65 which occurs at pH 7, Table 1). We furthermore investigated the condition in which α varies from 0 to 1 with particle/aggregate size according to varying DLVO interaction energies, using a fixed-PSD initial condition (approach C, Table 1). The results (Fig. S8 and Table S3) show that for cases of IS higher than 5 mM and for various pH, mean model fit R^2 is rather lower than that of previous approaches—0.687 and 0.429 for D_H and DCR, respectively. Although this approach could fit experimental data cases at 5, 7.5, and 10 mM CaCl_2 , with only one adjustable parameter (D_f), there was a need for adding another adjustable parameter in other cases, due probably to uncertainties in measurement of factors like zeta potential (with common accuracy on the order of $\pm 10\%$)⁷⁷ as reported in Fig. S9 and Table S3. Even considering two adjustable parameters (D_f and zeta potential), approach C was still unable to fit the case at 3 mM CaCl_2 . Other non-DLVO factors such as specific-ion effects⁷⁸ which have not been considered in this study or some basic assumptions of the DLVO such as perfect sphere⁷⁹ ignored for nonuniform-shaped porous aggregates might be reasons for the discrepancies.

Conventionally, open aggregate structures (D_f tends to 1.8) are formed in DLA regime where every contact results in attachment, while more compacted structures (D_f tends to 2.1) are formed under the more selective RLA condition.^{17, 80} As shown in Table 1, models fitted across both early and late stage data indicate that at CaCl_2 concentrations ≤ 3 mM (RLA) D_f is lower than 1.8 while at ≥ 5 mM (DLA) D_f ranges is higher than 2.03 and further increases with pH (up to 2.7 at pH 11). Approach B yielded even larger D_f on average by 11% compared to approach A. This difference was 8% for approach C. Strongly overlapping ranges of D_f for RLA and DLA regimes have been frequently reported in the literature,^{47, 81-85} especially for particles subject to mechanisms other than Brownian diffusion, such as ‘ballistic’ aggregation,¹⁷ orthokinetic aggregation,^{81, 86} and differential sedimentation.¹⁹ These can be the result of linear trajectories¹⁷ or restructuring.^{19, 41} It has also been indicated in the literature^{87,}

⁸⁸ that rapid particle-cluster aggregation leads to a denser aggregate ($D_f=2.5$) than cluster-cluster aggregation ($D_f=1.8$). Allain et al.¹⁹ reported a D_f value of 2.2 for calcium carbonate colloids within the DLA regime under quiescent sedimentation, and others⁸⁶ reported D_f in range of 2.3 to 2.8 for calcium phosphate in a system with settling and shear. Experimentally-measured D_f reported in the literature are typically limited to the early stage of aggregation or lower aggregation rates than those investigated in the present study.

Fitting the model to only the early stage of experiments showed ranges of D_f consistent with conventional expectations (Table S5) under the DLA regime. The contrasting trends obtained when fitting to both stages together suggests the crucial role of late-stage aggregation process in modifying this parameter. Our observation of an increase in the DCR curves under the RLA regime versus decreasing DCR in the DLA regime indicates that sedimentation under the RLA regime is slower than that under the DLA regime (Fig. 1c). This implies that the bulk density and therefore D_f of aggregates in the RLA regime should be lower than that under the DLA condition.

We deduce that in the late stage, evolved aggregates formed from mixed particle-cluster populations under the RLA condition are less compact than early-stage aggregates, potentially as a result of irregular packing geometries and inaccessibility of internal pore spaces to incident particles in unfavourable interaction conditions.⁸⁹ Decreasing D_f over the course of experiments has been observed already for fullerene NP under both DLA and RLA regimes.⁹⁰ However, due to uncertainties associated with the DCR data obtained under the RLA regime (discussed below), further experimental/modelling investigations are required to confirm this explanation. Conversely, aggregates formed in late-stage DLA conditions may have higher D_f (compared to less-compact early stage aggregates) as a result of internal reorganisation of particles within each aggregate, aggregate-aggregate collisions, and trapping individual particles in voids of

large, open clusters during their downward sedimentation.^{19, 89} It should be mentioned that model-fit parameter values might bear both experimental and model uncertainties. Direct experimental measurement of D_f under the late-stage conditions used in this study is a priority for future work to confirm the model predictions reported here.

Although all three modelling approaches are reasonably successful in fitting the experimental data, none of final models does so while maintaining all parameter values simultaneously within the ranges expected from previous literature. The model formulation applied in the present study is not able to reproduce the experimentally observed rise in DCR data under the RLA regime, because the sedimentation term used in these models is a simple decay term (last term in Eqs. 1,3) which avoids the computational expense and potential numerical dispersion problems of solving a spatio-temporal partial-differential equation.⁹¹ Although it was shown that DCR is an appropriate indicator of the mass concentration under DLA, it remains for future studies to validate this conclusion under the RLA regime. The modelled PSDs are shown in Figs. S2 and S3 and discussed in detail in the SI. Overall, approach B demonstrates the best overall match between observed PSD and modelled PSD through late-stage conditions.

Mass removal rates and measurement depth

Table 1 shows the predicted mean percentage mass removal after 5 h within a 3 cm modelled water column for different pH and IS, using parameter values estimated in both early and late stages. Under the RLA regime (2.5 and 3 mM CaCl_2) a negligible ($\leq 0.5\%$) decrease in mass concentration indicates that sedimentation is minimal, in agreement with our experimental observations (Fig 1c). Under the DLA regime (5-10 mM CaCl_2) and at various pH, for the three approaches A, B and C predicted mass removal reaches 85.4%, 74.5%, and 71.0%, respectively. Figure 3 shows that predicted mass removal is greater in the upper part of the water column. Removal percentage is maximum at pH 7 (86.4%, average of the three modelling

approaches, Table 1). With increasing pH above pH 7, mass removal decreases (down to 63.6% on average), consistent with the decrease of α and increase of D_f (Table 1). Surprisingly, as illustrated in Fig. 3 under the DLA condition, the percentage mass removal consistently (under almost all modelling approaches) decreases with increase in the IS from on average 79.5% at 5 mM CaCl_2 to 78.3% and 68.9% at 7.5 and 10 mM CaCl_2 , respectively (Table 1, Fig. 3).

We examined experimentally how the depth of measurement from the surface of the liquid affects the parameter values obtained using approach A. The results for depths of 0.33, 2.33, and 3.33 cm are presented in Table S6 and Fig. S10. For measurements at short distance below the water surface (0.33 cm), the aggregation is significantly lower than when measured at greater depths (2.33 and 3.33 cm). This might indicate the significance of differential sedimentation in aggregation of HAp NP. This also indicates that the late stage of coupled aggregation-sedimentation processes is less noticeable in the regions just below the surface of water. The model fit results (Table S6) confirm that late-stage influences on both α and D_f increase with the measurement depth. Crucially, α determined for the smallest depth (0.33 cm) assumes a value lower than one and D_f is relatively closer to the common threshold of DLA regime which agrees with fit result of early stage alone (Table S5). This strongly associates parameter values $\alpha > 1$ and D_f outside expected ranges of DLA regime, with the complications of interacting late-stage processes during coupled aggregation and sedimentation.

Implications for the fate of NP in groundwater and aquatic environments

The combination of experiment and modelling approaches presented here has enabled the complex interactions between aggregation and sedimentation to be investigated in NP systems well inside the late-stage at which the particle-aggregate population has evolved significantly from its initial PSD. These conditions are likely to be the norm in most environmental systems in which NP have been resident for any length of time. We demonstrate that population balance

models can be applied to systems at both stages of aggregate evolution. Although the best-performing model suite included permeability-based models for describing collision frequencies, the empirical, density-controlled descriptions for settling velocity were able to better describe the observed trends in experimental data over 5 h of coupled aggregation and sedimentation. Allowing the attachment efficiency to vary with aggregate size did not significantly alter model outcomes compared to assumption of a constant attachment efficiency, but fitted parameters were much more sensitive to the specification of the initial PSD. In terms of reduction in computational effort over the late-stage of the processes, we found the FP aggregation model has a greater capability than the MP technique. These results have significance in developing practical, computationally-efficient models for the fate and transport of NP in the environment.

While models fitted to only early stage data showed trends in attachment efficiency and fractal dimension consistent with classical theory, these trends varied as the systems evolved. Our results demonstrate that at lower IS (RLA), aggregation is slow, and sedimentation is negligible in the timescales considered here. At intermediate IS (5 mM CaCl_2) near the CCC, a moderate-rate DLA develops a population of NP clusters which are optimally more efficient at collecting (by aggregation) and removing (by sedimentation) large numbers of smaller particles and aggregates than that at higher IS (7.5 and 10 mM CaCl_2) where the system moves rapidly to fewer, larger, but less-compact aggregates, and overall mass removal rates are reduced due to slower sedimentation. These lower removal rates within high-IS solutions may bring about lifetimes and potential transport distances of NP aggregates in aqueous suspension in settings such as marine environments, coastal aquifers, or in soil pore microenvironments that are longer than expected based on conventional models or extrapolations from experimental data obtained only in early-stage conditions. Although the population balance techniques applied in the present study alleviate computational expenses of using an arithmetic particle size

discretization well with a geometric discretization when applied to small-scale laboratory conditions, it remains a question whether such models are efficient when coupled to fate and transport models at larger environmental scales, e.g., aquifer and watershed.

Supporting Information.

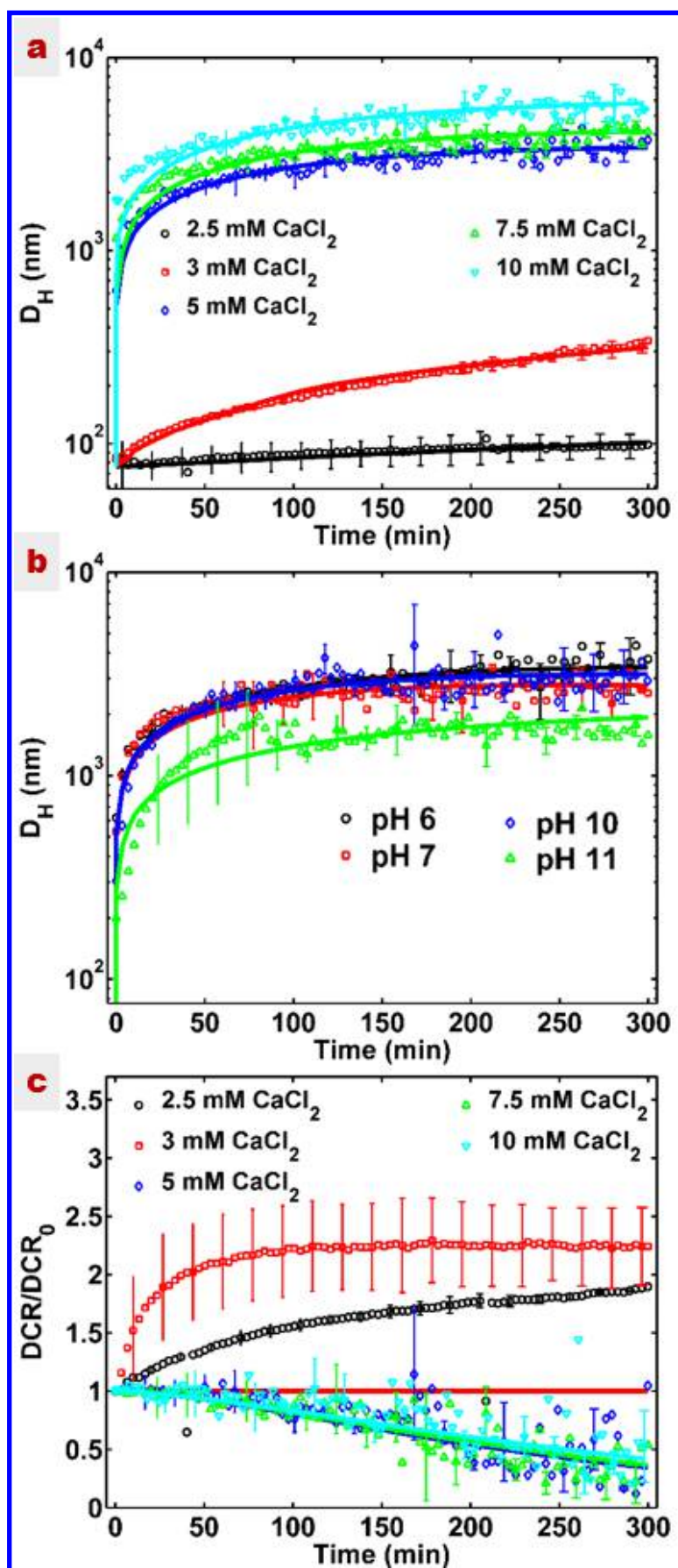
PDF File: Full model equations; details of MATLAB code; DVLO calculations and results; development of the parameter estimation algorithm; results of the comparison between numerical and analytical solutions; further investigations of sedimentation models; fit results to PSD; graphs of approaches B and C, etc.

Electronic Supporting Information: MATLAB codes developed for solution of FP and MP techniques and for parameter estimation of population balance models

Acknowledgements

Financial support from the University of Liverpool and National Tsing Hua University to PB through Dual-PhD programme is acknowledged. This work was also funded by the Taiwan's Ministry of Science and Technology (MOST) under the grant No. 104-2221-E-009-020-MY3 and by Sheffield Hallam University through an allocation of research time to JWB. We gratefully acknowledge Chien-Hou Wu and Chung-Yi Wu for providing full-time access to the DLS instrument. We gratefully acknowledge constructive suggestions from four anonymous reviewers and the editor in significantly improving this paper.

Figures and Tables



490 **Figure 1.** Evolution of averaged hydrodynamic diameter, D_H , (a,b) and change in mean

derived count rate (DCR) normalized to the initial derived count rate (DCR₀) (c) for HAp NPs at the point of measurement at various IS with a fixed pH at 6 (a,c) and various pH with a fixed IS at 5 mM CaCl₂ (b). The model used here was FP with power law formulation and Brinkman collision model. The modelling approach includes a fixed initial PSD with considering the pre-early stage of aggregation and a constant attachment efficacy (approach B).

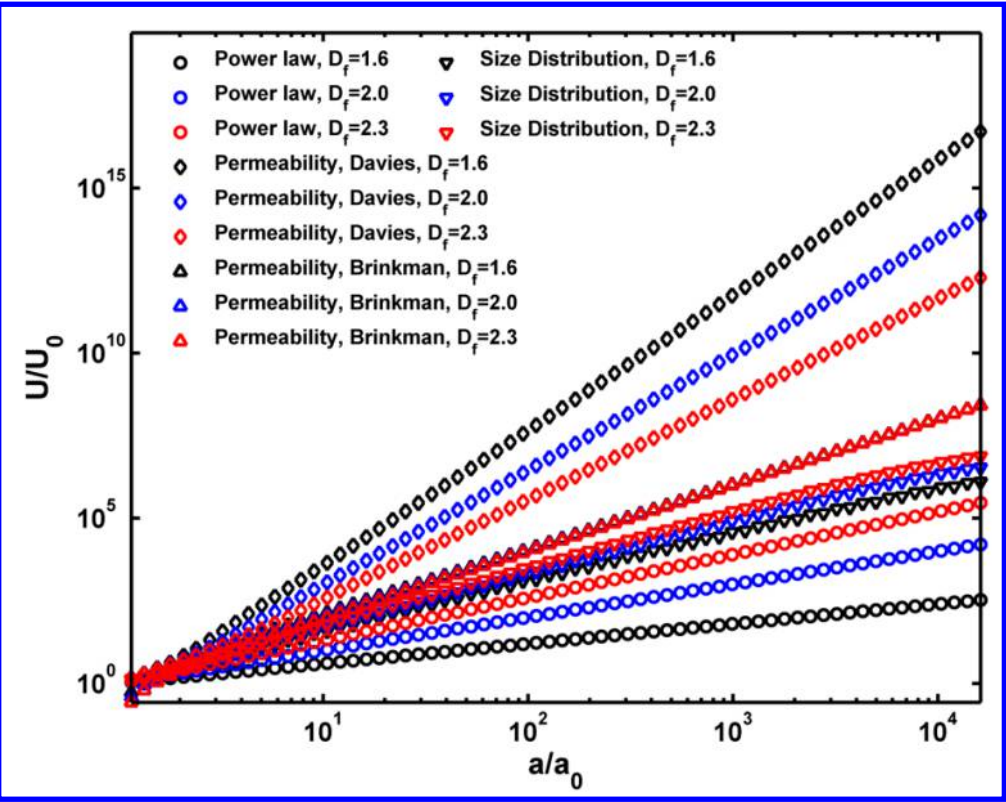
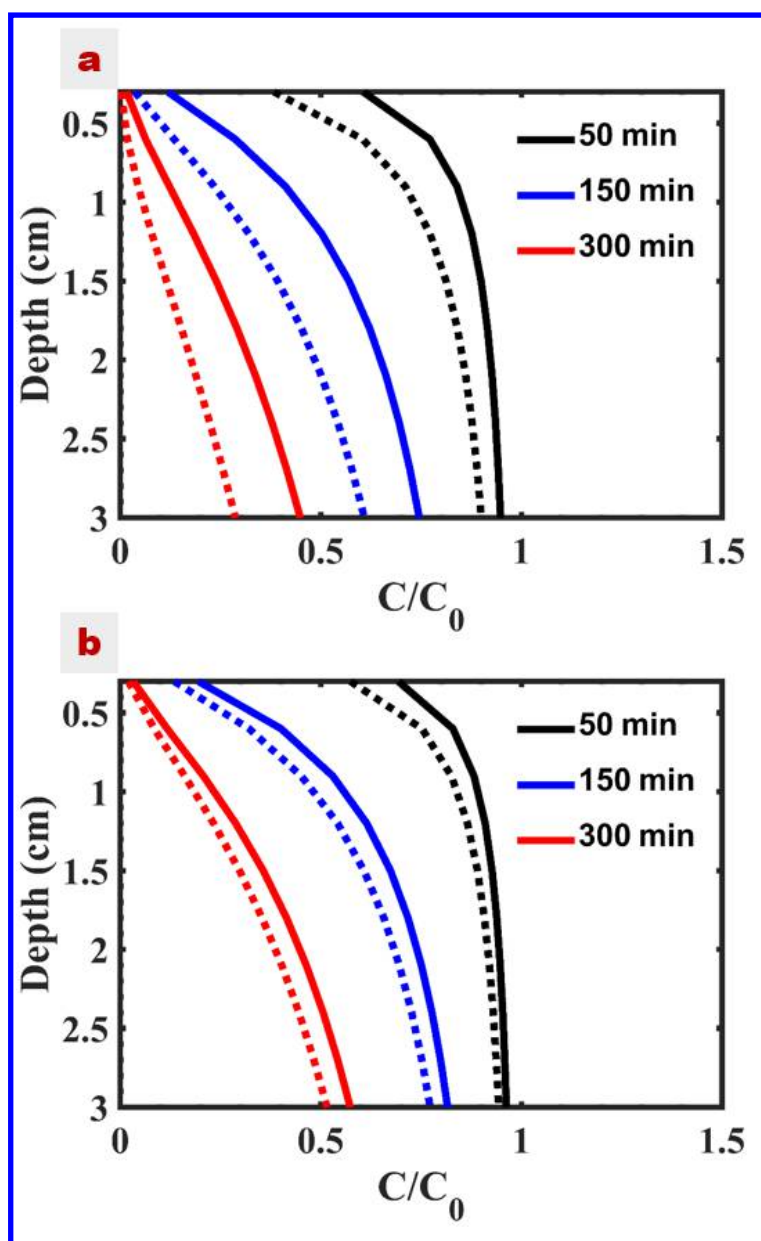


Figure 2. Trends of settling velocity, U , normalized to the settling velocity of primary particles, U_0 , versus particle radius of each size class, a , normalized by the primary particle radius (smallest size class), a_0 , calculated by four different types of velocity models. Fractal dimension is set as 1.6, 2, and 2.3. The primary particle radius used in these models is 40 nm.

503



504 **Figure 3.** Modelled mass concentration, C , profiles normalized by the initial mass
 505 concentration, C_0 , versus the water column depth at (a) 5 mM CaCl_2 and (b) 10 mM CaCl_2 after
 506 50, 150, and 300 min. The continuous lines represent approach A (case-specific initial PSD)
 507 and dashed lines represent approach C (fixed initial PSD combined with variable α computed
 508 by DLVO).

509

510

511 **Table 1.** Model parameters estimated by fitting FP models to both early and late stages of
512 aggregation under different electrolyte concentrations (at fixed pH 6) and different pH (at fixed
513 electrolyte concentration, 5 mM CaCl₂) over 5 h, based on three modelling approaches (A, B,
514 C), and mass removal results estimated by the models for a sample volume of 3 mL (3 cm water
515 depth) after 5 h. The power-law model and Brinkman-based permeability model are used to
516 calculate the sedimentation velocity and collision frequencies, respectively.

Parameter	Modelling approach	Electrolyte Concentration (mM)					pH		
		2.5	3	5	7.5	10	7	10	11
α	A	1.1×10 ⁻⁴	7.1×10 ⁻³	11.60	8.10	1.10	15.40	6.33	1.59
	B	2.0×10 ⁻⁶	1.0×10 ⁻⁵	1.13	1.13	1.23	1.65	1.37	0.21
	C	NA	NA	NA	NA	NA	NA	NA	NA
D _r	A	1.53	1.48	2.03	2.12	2.27	2.26	2.32	2.70
	B	1.71	1.38	2.53	2.53	2.45	2.69	2.63	2.66
	C	1.50	1.50	2.50	2.42	2.25	2.60	2.61	2.70
Removal %	A	0.4	1.0	86.1	86.9	70.0	94.9	88.8	84.7
	B	0.1	0.1	77.5	75.8	71.8	86.3	81.6	50.9
	C	0.1	0.1	75.0	72.2	65.0	78.0	76.8	55.1

517 A: initial PSD; B: identical PSD; C: identical PSD, DLVO; NA: not applicable

518

519

References

1. Wang, D.; Jin, Y.; Jaisi, D., Cotransport of Hydroxyapatite Nanoparticles and Hematite Colloids in Saturated Porous Media: Mechanistic Insights from Mathematical Modeling and Phosphate Oxygen Isotope Fractionation. *J. Contam. Hydrol.* **2015**, *182*, 194-209.
2. Fuller, C.; Bargar, J.; Davis, J.; Piana, M., Mechanisms of uranium interactions with hydroxyapatite: Implications for groundwater remediation. *Environ. Sci. Technol.* **2002**, *36*, (2), 158-165.
3. Kanel, S. R.; Clement, T. P.; Barnett, M. O.; Goltz, M. N., Nano-Scale Hydroxyapatite: Synthesis, Two-Dimensional Transport Experiments, and Application for Uranium Remediation. *J. of Nanotechnol.* **2011**, *2011*, 1-5.
4. Babakhani, P.; Bridge, J.; Doong, R.-a.; Phenrat, T., Continuum-based models and concepts for the transport of nanoparticles in saturated porous media: A state-of-the-science review. *Adv. Colloid Interface Sci.* **2017**, *246*, (Supplement C), 75-104.
5. Babakhani, P.; Bridge, J.; Doong, R.-a.; Phenrat, T., Parameterization and prediction of nanoparticle transport in porous media: A reanalysis using artificial neural network. *Water Resour. Res.* **2017**, *53*, 4564-4585.
6. McCarthy, J. F.; Zachara, J. M., Subsurface transport of contaminants. *Environ. Sci. Technol.* **1989**, *23*, (5), 496-502.
7. Kersting, A. B.; Efur, D. W.; Finnegan, D. L.; Rokop, D. J.; Smith, D. K.; Thompson, J. L., Migration of plutonium in ground water at the Nevada Test Site. *Nature* **1999**, *397*, (6714), 56-59.
8. Kansanen, P. H.; Jaakkola, T.; Kulmala, S.; Suutarinen, R., Sedimentation and distribution of gamma-emitting radionuclides in bottom sediments of southern Lake Päijänne, Finland, after the Chernobyl accident. *Hydrobiologia* **1991**, *222*, (2), 121-140.
9. Evangeliou, N.; Florou, H., The dispersion of 137 Cs in a shallow Mediterranean embayment (Saronikos Gulf–Elefsis Bay), estimated inventories and residence times. *J. Environ. Radioact.* **2012**, *113*, 87-97.
10. Otosaka, S.; Kobayashi, T., Sedimentation and remobilization of radiocesium in the coastal area of Ibaraki, 70 km south of the Fukushima Dai-ichi Nuclear Power Plant. *Environ. Monit. Assess.* **2013**, *185*, (7), 5419-5433.
11. Babakhani, P.; Fagerlund, F.; Shamsai, A.; Lowry, G. V.; Phenrat, T., Modified MODFLOW-based model for simulating the agglomeration and transport of polymer-modified Fe nanoparticles in saturated porous media. *Environ Sci Pollut Res*, 1-20, doi:10.1007/s11356-015-5193-0 **2015**.
12. Phenrat, T.; Kim, H. J.; Fagerlund, F.; Illangasekare, T.; Tilton, R. D.; Lowry, G. V., Particle size distribution, concentration, and magnetic attraction affect transport of polymer-modified FeO nanoparticles in sand columns. *Environ. Sci. Technol.* **2009**, *43*, (13), 5079-5085.
13. Keller, A. A.; Wang, H.; Zhou, D.; Lenihan, H. S.; Cherr, G.; Cardinale, B. J.; Miller, R.; Ji, Z., Stability and aggregation of metal oxide nanoparticles in natural aqueous matrices. *Environ. Sci. Technol.* **2010**, *44*, (6), 1962-1967.
14. Phenrat, T.; Saleh, N.; Sirk, K.; Tilton, R. D.; Lowry, G. V., Aggregation and sedimentation of aqueous nanoscale zerovalent iron dispersions. *Environ. Sci. Technol.* **2007**, *41*, (1), 284-290.
15. Gambinossi, F.; Mylon, S. E.; Ferri, J. K., Aggregation kinetics and colloidal stability of functionalized nanoparticles. *Adv. Colloid Interface Sci.* **2015**, *222*, 332-349.

- 564 16. Szilagyi, I.; Szabo, T.; Desert, A.; Trefalt, G.; Oncsik, T.; Borkovec, M., Particle aggregation
565 mechanisms in ionic liquids. *PCCP* **2014**, *16*, (20), 9515-9524.
- 566 17. Elimelech, M.; Gregory, J.; Jia, X., *Particle deposition and aggregation: measurement,*
567 *modelling and simulation*. Butterworth-Heinemann: 1998.
- 568 18. Afshinnia, K.; Sikder, M.; Cai, B.; Baalousha, M., Effect of nanomaterial and media
569 physicochemical properties on Ag NM aggregation kinetics. *J. Colloid Interface Sci.* **2017**, *487*,
570 192-200.
- 571 19. Allain, C.; Cloitre, M.; Parisse, F., Settling by cluster deposition in aggregating colloidal
572 suspensions. *J. Colloid Interface Sci.* **1996**, *178*, (2), 411-416.
- 573 20. Lin, S.; Wiesner, M. R., Deposition of Aggregated Nanoparticles □ A Theoretical and
574 Experimental Study on the Effect of Aggregation State on the Affinity between Nanoparticles
575 and a Collector Surface. *Environ. Sci. Technol.* **2012**, *46*, (24), 13270-13277.
- 576 21. Afshinnia, K.; Gibson, I.; Merrifield, R.; Baalousha, M., The concentration-dependent
577 aggregation of Ag NPs induced by cystine. *Sci. Total Environ.* **2016**, *557*, 395-403.
- 578 22. Grolimund, D.; Elimelech, M.; Borkovec, M., Aggregation and deposition kinetics of mobile
579 colloidal particles in natural porous media. *Colloids Surf. A* **2001**, *191*, (1-2), 179-188.
- 580 23. Westerhoff, P.; Nowack, B., Searching for global descriptors of engineered nanomaterial fate
581 and transport in the environment. *Acc. Chem. Res.* **2012**, *46*, (3), 844-853.
- 582 24. Zhang, W., Nanoparticle aggregation: principles and modeling. In *Nanomaterial Impacts on Cell*
583 *Biology and Medicine*, David G. Capco, Y. C., Ed. Springer: 2014; pp 19-43.
- 584 25. Smoluchowski, M., Versuch einer mathematischen Theorie der Koagulationskinetik kolloider
585 Lösungen. *Zeitschrift fuer Physikalische Chemie.* **1917**, *92*, 129-68.
- 586 26. Chandrasekhar, S., Stochastic problems in physics and astronomy. *Reviews of modern physics*
587 **1943**, *15*, (1), 1.
- 588 27. Rigopoulos, S., Population balance modelling of polydispersed particles in reactive flows. *Prog.*
589 *Energy Combust. Sci.* **2010**, *36*, (4), 412-443.
- 590 28. Ramkrishna, D., *Population balances: Theory and applications to particulate systems in*
591 *engineering*. Academic press: 2000.
- 592 29. Ramkrishna, D.; Singh, M. R., Population balance modeling: current status and future prospects.
593 *Annu. Rev. Chem. Biomol. Eng.* **2014**, *5*, 123-146.
- 594 30. Hounslow, M. J.; Ryall, R. L.; Marshall, V. R., A discretized population balance for nucleation,
595 growth, and aggregation. *AIChE J.* **1988**, *34*, (11), 1821-1832.
- 596 31. Lister, J.; Smit, D.; Hounslow, M., Adjustable discretized population balance for growth and
597 aggregation. *AIChE J.* **1995**, *41*, (3), 591-603.
- 598 32. Dale, A. L.; Lowry, G. V.; Casman, E. A., Accurate and fast numerical algorithms for tracking
599 particle size distributions during nanoparticle aggregation and dissolution. *Environ. Sci. Nano*
600 **2017**, *4*, (1), 89-104.
- 601 33. Kumar, S.; Ramkrishna, D., On the solution of population balance equations by discretization—
602 I. A fixed pivot technique. *Chem. Eng. Sci.* **1996**, *51*, (8), 1311-1332.
- 603 34. Kumar, S.; Ramkrishna, D., On the solution of population balance equations by discretization—
604 II. A moving pivot technique. *Chem. Eng. Sci.* **1996**, *51*, (8), 1333-1342.
- 605 35. Thill, A.; Moustier, S.; Aziz, J.; Wiesner, M. R.; Bottero, J. Y., Flocs restructuring during
606 aggregation: experimental evidence and numerical simulation. *J. Colloid Interface Sci.* **2001**,
607 *243*, (1), 171-182.

36. Quik, J. T. K.; Velzeboer, I.; Wouterse, M.; Koelmans, A. A.; Van de Meent, D., Heteroaggregation and sedimentation rates for nanomaterials in natural waters. *Water Res.* **2014**, *48*, 269-279.
37. Markus, A. A.; Parsons, J. R.; Roex, E. W. M.; de Voogt, P.; Laane, R., Modeling aggregation and sedimentation of nanoparticles in the aquatic environment. *Sci. Total Environ.* **2015**, *506*, 323-329.
38. Hunt, J. R., Self-similar particle-size distributions during coagulation: theory and experimental verification. *J. Fluid Mech.* **1982**, *122*, 169-185.
39. Veerapaneni, S.; Wiesner, M. R., Hydrodynamics of fractal aggregates with radially varying permeability. *J. Colloid Interface Sci.* **1996**, *177*, (1), 45-57.
40. Vikesland, P. J.; Rebodos, R. L.; Bottero, J. Y.; Rose, J.; Masion, A., Aggregation and sedimentation of magnetite nanoparticle clusters. *Environ. Sci. Nano* **2016**, *3*, (3), 567-577.
41. Jeldres, R. I.; Concha, F.; Toledo, P. G., Population balance modelling of particle flocculation with attention to aggregate restructuring and permeability. *Adv. Colloid Interface Sci.* **2015**, *224*, 62-71.
42. Li, X.-Y.; Logan, B. E., Permeability of fractal aggregates. *Water Res.* **2001**, *35*, (14), 3373-3380.
43. Johnson, C. P.; Li, X.; Logan, B. E., Settling Velocities of Fractal Aggregates. *Environ. Sci. Technol.* **1996**, *30*, (6), 1911-1918.
44. Aziz, J. J.; Serra, C. A.; Wiesner, M. R., Hydrodynamics of permeable aggregates in differential sedimentation. *Environ. Eng. Sci.* **2003**, *20*, (1), 21-31.
45. Therezien, M.; Thill, A.; Wiesner, M. R., Importance of heterogeneous aggregation for NP fate in natural and engineered systems. *Sci. Total Environ.* **2014**, *485*, 309-318.
46. Li, D. H.; Ganczarczyk, J., Fractal geometry of particle aggregates generated in water and wastewater treatment processes. *Environ. Sci. Technol.* **1989**, *23*, (11), 1385-1389.
47. Sterling, M. C.; Bonner, J. S.; Ernest, A. N. S.; Page, C. A.; Autenrieth, R. L., Application of fractal flocculation and vertical transport model to aquatic sol-sediment systems. *Water Res.* **2005**, *39*, (9), 1818-1830.
48. Logan, B. E.; Hunt, J. R., Advantages to microbes of growth in permeable aggregates in marine systems. *Limnol. Oceanogr* **1987**, *32*, (5), 1034-1048.
49. Vahedi, A.; Gorczyca, B., Settling velocities of multifractal flocs formed in chemical coagulation process. *Water Res.* **2014**, *53*, 322-328.
50. Khelifa, A.; Hill, P. S., Models for effective density and settling velocity of flocs. *J. Hydraul. Res.* **2006**, *44*, (3), 390-401.
51. Wang, D.; Bradford, S. A.; Harvey, R. W.; Gao, B.; Cang, L.; Zhou, D., Humic acid facilitates the transport of ARS-labeled hydroxyapatite nanoparticles in iron oxyhydroxide-coated sand. *Environ. Sci. Technol.* **2012**, *46*, (5), 2738-2745.
52. Jacobson, M. Z., *Fundamentals of atmospheric modeling*. Cambridge university press: 2005.
53. Nopens, I.; Beheydt, D.; Vanrolleghem, P. A., Comparison and pitfalls of different discretised solution methods for population balance models: a simulation study. *Comput. Chem. Eng.* **2005**, *29*, (2), 367-377.
54. Lee, K. W.; Lee, Y. J.; Han, D. S., The log-normal size distribution theory for Brownian coagulation in the low Knudsen number regime. *J. Colloid Interface Sci.* **1997**, *188*, (2), 486-492.
55. Nash, J. E.; Sutcliffe, J. V., River flow forecasting through conceptual models part I — A discussion of principles. *J. Hydrol.* **1970**, *10*, (3), 282-290.

- 654 56. Wallace, S. J.; Li, J.; Nation, R. L.; Boyd, B. J., Drug release from nanomedicines: selection of
655 appropriate encapsulation and release methodology. *Drug Deliv. Transl. Res.* **2012**, 2, (4), 284-
656 292.
- 657 57. Missana, T.; Alonso, U.; Albarran, N.; García-Gutiérrez, M.; Cormenzana, J.-L., Analysis of
658 colloids erosion from the bentonite barrier of a high level radioactive waste repository and
659 implications in safety assessment. *Phys. Chem. Earth. A/B/C* **2011**, 36, (17), 1607-1615.
- 660 58. Holmboe, M.; Wold, S.; Jonsson, M.; Garcia-Garcia, S., Effects of γ -irradiation on the stability
661 of colloidal Na⁺-Montmorillonite dispersions. *Appl. Clay Sci.* **2009**, 43, (1), 86-90.
- 662 59. Song, D.; Jin, H.; Jin, J.; Jing, D., Sedimentation of particles and aggregates in colloids
663 considering both streaming and seepage. *J. Phys. D: Appl. Phys.* **2016**, 49, (42), 425303.
- 664 60. Byun, J.; Son, M.; Yang, J.-S.; Jung, T.-H., Volumetric concentration maximum of cohesive
665 sediment in waters: A numerical study. *Water* **2014**, 7, (1), 81-98.
- 666 61. Brom, v. d. Aggregation of gold clusters by complementary hydrogen bonding. University of
667 Groningen, 2006.
- 668 62. García-García, S.; Wold, S.; Jonsson, M., Kinetic determination of critical coagulation
669 concentrations for sodium-and calcium-montmorillonite colloids in NaCl and CaCl₂
670 aqueous solutions. *J. Colloid Interface Sci.* **2007**, 315, (2), 512-519.
- 671 63. García-García, S.; Jonsson, M.; Wold, S., Temperature effect on the stability of bentonite
672 colloids in water. *J. Colloid Interface Sci.* **2006**, 298, (2), 694-705.
- 673 64. Baalousha, M.; Nur, Y.; Römer, I.; Tejamaya, M.; Lead, J. R., Effect of monovalent and divalent
674 cations, anions and fulvic acid on aggregation of citrate-coated silver nanoparticles. *Sci. Total*
675 *Environ.* **2013**, 454, 119-131.
- 676 65. Tomaszewska, E.; Soliwoda, K.; Kadziola, K.; Tkacz-Szczesna, B.; Celichowski, G.; Cichomski,
677 M.; Szmaja, W.; Grobelny, J., Detection limits of DLS and UV-Vis spectroscopy in
678 characterization of polydisperse nanoparticles colloids. *J Nanomater.* **2013**, 2013, 60.
- 679 66. Bushell, G. C.; Yan, Y. D.; Woodfield, D.; Raper, J.; Amal, R., On techniques for the
680 measurement of the mass fractal dimension of aggregates. *Adv. Colloid Interface Sci.* **2002**, 95,
681 (1), 1-50.
- 682 67. Li, X.; Logan, B. E., Collision frequencies of fractal aggregates with small particles by
683 differential sedimentation. *Environ. Sci. Technol.* **1997**, 31, (4), 1229-1236.
- 684 68. Vahedi, A.; Gorczyca, B., Predicting the settling velocity of flocs formed in water treatment
685 using multiple fractal dimensions. *Water Res.* **2012**, 46, (13), 4188-4194.
- 686 69. Jin, B.; Wilén, B.-M.; Lant, P., A comprehensive insight into floc characteristics and their impact
687 on compressibility and settleability of activated sludge. *Chem. Eng. J.* **2003**, 95, (1), 221-234.
- 688 70. Lee, D. J.; Chen, G. W.; Liao, Y. C.; Hsieh, C. C., On the free-settling test for estimating
689 activated sludge floc density. *Water Res.* **1996**, 30, (3), 541-550.
- 690 71. Risovic, D.; Martinis, M., The role of coagulation and sedimentation mechanisms in the two-
691 component model of sea-particle size distribution. *Fizika* **1994**, 3, (2), 103-118.
- 692 72. Emadzadeh, A.; Chiew, Y. M., Settling velocity of a porous sphere. In *River Flow 2016*, CRC
693 Press: 2016; pp 555-562.
- 694 73. Metreveli, G.; Frombold, B.; Seitz, F.; Grün, A.; Philippe, A.; Rosenfeldt, R. R.; Bundschuh, M.;
695 Schulz, R.; Manz, W.; Schaumann, G. E., Impact of chemical composition of ecotoxicological
696 test media on the stability and aggregation status of silver nanoparticles. *Environ. Sci. Nano*
697 **2016**, 3, (2), 418-433.

74. Zhang, W.; Crittenden, J.; Li, K.; Chen, Y., Attachment efficiency of nanoparticle aggregation in aqueous dispersions: modeling and experimental validation. *Environ. Sci. Technol.* **2012**, *46*, (13), 7054-7062.
75. Logan, B. E.; Jewett, D. G.; Arnold, R. G.; Bouwer, E. J.; O'Melia, C. R., Clarification of clean-bed filtration models. *J. Environ. Eng.* **1995**, *121*, (12), 869-873.
76. Martin, M. J.; Logan, B. E.; Johnson, W. P.; Jewett, D. G.; Arnold, R. G., Scaling bacterial filtration rates in different sized porous media. *J. Environ. Eng.* **1996**, *122*, (5), 407-415.
77. Lowry, G. V.; Hill, R. J.; Harper, S.; Rawle, A. F.; Hendren, C. O.; Klaessig, F.; Nobbmann, U.; Sayre, P.; Rumble, J., Guidance to improve the scientific value of zeta-potential measurements in nanoEHS. *Environ. Sci. Nano* **2016**, *3*, (5), 953-965.
78. Oncsik, T.; Trefalt, G.; Borkovec, M.; Szilagyi, I., Specific ion effects on particle aggregation induced by monovalent salts within the Hofmeister series. *Langmuir* **2015**, *31*, (13), 3799-3807.
79. Baalousha, M., Effect of nanomaterial and media physicochemical properties on nanomaterial aggregation kinetics. *NanoImpact* **2017**, *6*, 55-68.
80. Chowdhury, I.; Walker, S. L.; Mylon, S. E., Aggregate morphology of nano-TiO₂: role of primary particle size, solution chemistry, and organic matter. *Environ. Sci. Process Impacts* **2013**, *15*, (1), 275-282.
81. Jiang, Q.; Logan, B. E., Fractal dimensions of aggregates determined from steady-state size distributions. *Environ. Sci. Technol.* **1991**, *25*, (12), 2031-2038.
82. Potenza, M. A. C.; Manca, A.; Veen, S. J.; Weber, B.; Mazzoni, S.; Schall, P.; Wegdam, G. H., Dynamics of colloidal aggregation in microgravity by critical Casimir forces. *EPL (Europhysics Letters)* **2014**, *106*, (6), 68005.
83. Schaefer, D. W.; Martin, J. E.; Wiltzius, P.; Cannell, D. S., Fractal geometry of colloidal aggregates. *Phys. Rev. Lett.* **1984**, *52*, (26), 2371.
84. Zhang, J. j.; Li, X. y., Modeling particle-size distribution dynamics in a flocculation system. *AIChE J.* **2003**, *49*, (7), 1870-1882.
85. Lee, B. J.; Molz, F., Numerical simulation of turbulence-induced flocculation and sedimentation in a flocculant-aided sediment retention pond. *Environmental Engineering Research* **2014**, *19*, (2), 165-174.
86. Tang, P.; Greenwood, J.; Raper, J. A., A model to describe the settling behavior of fractal aggregates. *J. Colloid Interface Sci.* **2002**, *247*, (1), 210-219.
87. Hanus, L. H.; Hartzler, R. U.; Wagner, N. J., Electrolyte-induced aggregation of acrylic latex. 1. Dilute particle concentrations. *Langmuir* **2001**, *17*, (11), 3136-3147.
88. Russel, W. B.; Saville, D. A.; Schowalter, W. R., *Colloidal dispersions*. Cambridge university press: 1989.
89. Meng, Z.; Hashmi, S. M.; Elimelech, M., Aggregation rate and fractal dimension of fullerene nanoparticles via simultaneous multiangle static and dynamic light scattering measurement. *J. Colloid Interface Sci.* **2013**, *392*, 27-33.
90. González, A. E., Colloidal Aggregation Coupled with Sedimentation: A Comprehensive Overview. In *Advances in Colloid Science*, InTech: 2016.
91. Zheng, C.; Wang, P. P., A modular three-dimensional multi-species transport model for simulation of advection, dispersion and chemical reactions of contaminants in groundwater systems; documentation and user's guide. *US Army Engineer Research and Development Center Contract Report SERDP-99-1, Vicksburg, Mississippi, USA* **1999**.